# Power-Electronics-Based Solutions for Plug-in Hybrid Electric Vehicle Energy Storage and Management Systems

Zahra Amjadi, *Student Member, IEEE*, and Sheldon S. Williamson, *Member, IEEE*

***Abstract*—Batteries, ultracapacitors (UCs), and fuel cells are widely being proposed for electric vehicles (EVs) and plug-in hybrid EVs (PHEVs) as an electric power source or an energy storage unit. In general, the design of an intelligent control strategy for coordinated power distribution is a critical issue for UC-supported PHEV power systems. Implementation of several control methods has been presented in the past, with the goal of improving battery life and overall vehicle efficiency. It is clear that the control objectives vary with respect to vehicle velocity, power demand, and state of charge of both the batteries and UCs. Hence, an optimal control strategy design is the most critical aspect of an all-electric/plug-in hybrid electric vehicle operational characteristic. Although much effort has been made to improve the life of PHEV energy storage systems (ESSs), including research on energy storage device chemistries, this paper, on the contrary, highlights the fact that the fundamental problem lies within the design of power-electronics-based energy-management converters and the development of smarter control algorithms. This paper initially discusses battery and UC characteristics and then goes on to provide a detailed comparison of various proposed control strategies and proposes the use of precise power electronic converter topologies. Finally, this paper summarizes the benefits of the various techniques and suggests the most viable solutions for on-board power management, more specific to PHEVs with multiple/hybrid ESSs.**

***Index Terms*—Battery storage, capacitors, electric vehicles (EVs), energy management, energy storage, power electronics, road vehicles.**

## I. Introduction

THE INCREASING popularity of electric vehicles (EVs) and plug-in hybrid electric vehicles (PHEVs) is attributed to the savings in fuel costs compared to conventional internal combustion engine (ICE) vehicles. EVs and PHEVs save energy due to the employment of reverse regenerating braking during the deceleration cycle. This energy is typically stored in batteries and ultracapacitors (UCs). The incorporation of on-board energy storage systems (ESS) and generation in PHEVs has been facilitated and dictated by the market demands for enhanced performance and range. The ensuing sections will discuss battery and UC characteristics and series and parallel energy storage topologies. Furthermore, this paper will go on to discuss proposed control strategies, energy source models, and benefits of energy storage.

Manuscript received March 13, 2009; revised September 1, 2009. First published September 22, 2009; current version published January 13, 2010.

The authors are with the Power Electronics and Energy Research Group, Department of Electrical and Computer Engineering, Concordia University, Montreal, QC H3G 1M8, Canada (e-mail: sheldon@ece.concordia.ca).

Color versions of one or more of the figures in this paper are available online at http://ieeexplore.ieee.org.

Digital Object Identifier 10.1109/TIE.2009.2032195

### A. Battery and UC Characteristics

A battery is able to store large amounts of energy (on the order of 1 kW/kg; 100 W · h/kg) but is not suitable for supplying a large amount of power in a very short time due to low power output density. An increase in efficiency of energy source can be achieved by using a smaller battery with a lower peak output power. A UC has low storage capacity but possesses the ability to supply a large burst of power (on the order of 10 kW/kg; 1 W · h/kg). The battery is used to supply a large amount of power at light loads, thereby increasing the total efficiency, whereas the UC bank is used for satisfying acceleration and regenerative braking requirements. Such a scenario also helps improve the on-board battery lifetime. The combination of battery and UC results in reduced size and weight of the overall ESS. Together, a UC and a battery can combine to meet the storage and peak current characteristics. This is achieved by connecting two energy sources in a parallel configuration [1], [2].

### B. Series and Parallel Energy Storage Topologies

Three configurations of hybrid drive trains exist, namely, series, parallel, and series–parallel configurations. Due to the varying sizes of the drive trains and the availability of space on the vehicle, parallel and series–parallel hybrid drive trains are used in smaller passenger vehicles, while the series configuration is deemed suitable for larger vehicles. A combination of UC and battery results in a hybrid ESS (HESS) [3]–[15]. This configuration can be either passively or actively connected. An actively connected configuration requires power electronic components, which drive their costs upward. The actively connected HESS regulates the transfer of energy to and from each component and the system through a controllable power electronics buffer between the batteries and the UC. The advantage of HESS is that the overall mass of the system can be potentially smaller than that of a passive configuration for the same load. A parallel connection of battery and UC results in a simple configuration, as shown in Fig. 1.

Control overcharging and discharging of the components is limited in the parallel configuration. Parallel connected UC and battery have equal voltages across them. A dc/dc converter supplies the power demand of motor from the HESS, thus maintaining a constant voltage on the bus [3].

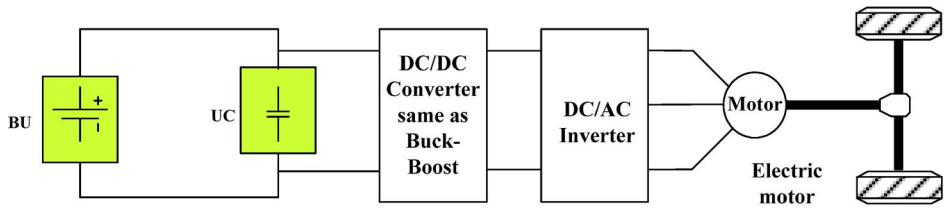


Fig. 1. Passive parallel connection topology.

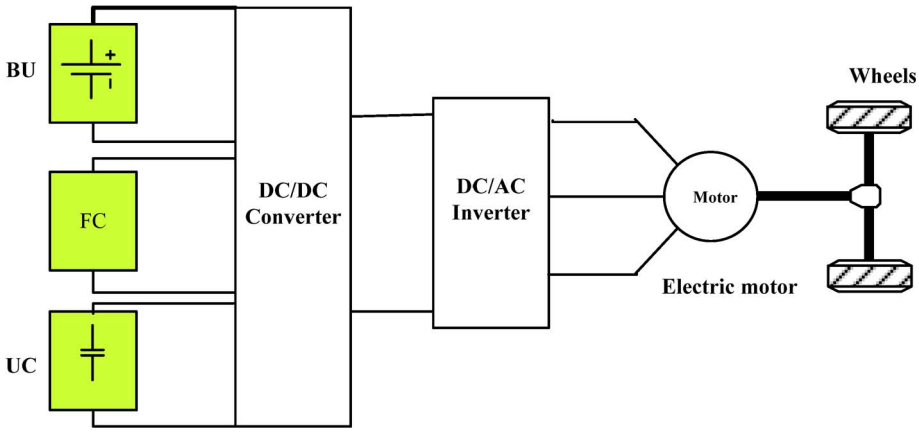


Fig. 2. Typical three-way HESS.

## II. Proposed Control Strategies for PHEV Energy Storage Systems

The arrangement for a typical three-way PHEV ESS consists of a regenerative fuel cell (RFC), a UC bank, and a battery unit system. The RFC generator acts as the main energy source but has a poor efficiency at light loads, thus relying on battery for energy requirements at lighter loads. A bidirectional step-up/step-down dc/dc converter, as shown in Fig. 2, connects each power source to the dc link.

As aforementioned, for transferring energy from each source to the dc link, a step-up mode of operation is used, while for charging both the UC bank and battery storage system and for recovering braking energy, the step-down operation is used [4]–[6].

### A. Multiple-Input Converter Topology

For achieving high efficiency, EV/PHEV traction drives are typically supplied at a high voltage, usually in the range of 300–600 V. A bidirectional topology is selected to allow the voltage levels to be changed as a function of load power requirement and, thus, is used to connect low power voltage sources. In the three-way battery, UC, and RFC generator system, the number of elements connected in series is limited to improve system reliability. The step-up/step-down converter consists of two controlled power electronic switches and two power diodes, while an input inductor and an output capacitor are used to limit the output current ripple of each power source. This arrangement minimizes the voltage ripple in the input terminal of the traction drive. A precharge circuit is used to avoid overcurrents at start-up [6], [7].

The state of charge (SOC) of UC and battery, the per-second maximum output current variation, and the efficiency map of the power sources define the current control strategy used for both RFC and battery. This gives an appropriate dynamic response during either acceleration or braking operation, along with the desired working point of RFC generator $V$–$I$ characteristic.

The RFC generator does not recover energy or provide high dynamic response, as large auxiliary devices are used to feed hydrogen and to accomplish the reforming process. The RFC source has a very low efficiency when the power supplied by it is in the 0%–15% range of its rated power. The RFC generator is operated only when the total power is higher than 15% of its rated power. Thus, a battery storage unit is combined with the RFC generator to balance the load power requirement to satisfy both efficiency and load dynamic specifications. The difference between the current required by the traction drive and the current supplied by the RFC system is delivered by the battery.

UCs have high power density, obtain regeneration energy at high efficiency during decelerations, and supply the stored energy during accelerations. A UC typically depicts low energy density, and it needs a battery to assist the RFC generator in supplying the traction drive during low dynamics. Battery lifetime and dynamic stress can be saved when UC supplies the power required in excess of the RFC–battery systems instantaneous capability. The system control algorithm includes suitable regulation of the SOC of battery and UC. The SOC value is maintained greater than the minimum allowable value [8], [9].

The power delivered by the UC can be calculated using the following equations:

$$P_{\text{discharge-UC}}(\text{SOC}) = V_{\min} \times \frac{V_{\text{OC}}(\text{SOC}) - V_{\min}}{R_{\text{discharge-UC}}(\text{SOC})} \quad (1)$$

where $V_{\min}$ and $V_{\max}$ are the voltages at full charge state or discharge state of the battery, respectively, and

$$R_{\text{discharge-UC}}(\text{SOC}) = \frac{V_{\text{OC-initial}}(\text{SOC}) - V_{\text{final}}(\text{SOC})}{I_{\text{load}}} \quad (2)$$

$$V_{\text{final}}(\text{SOC}) = V_{\text{OC-final}}(\text{SOC}) - IR_{\text{ohmic}} \quad (3)$$

$$V_{\text{OC}} = \frac{Q}{C}. \quad (4)$$

The discharge resistance for a UC ($R_{\text{discharge-UC}}$) depends on both the voltage drop and the fact that the SOC of the battery reduces drastically during discharge [3]. The UC equations in charge state are given by

$$P_{\text{charge-UC}}(\text{SOC}) = V_{\max} \times \frac{V_{\max} - V_{\text{OC}}(\text{SOC})}{R_{\text{charge-UC}}(\text{SOC})} \quad (5)$$

$$R_{\text{charge-UC}}(\text{SOC}) = \frac{V_{\text{final}}(\text{SOC}) - V_{\text{OC-initial}}(\text{SOC})}{I_{\text{load}}} \quad (6)$$

$$V_{\text{final}}(\text{SOC}) = V_{\text{OC-final}}(\text{SOC}) + \text{IR}_{\text{ohmic}}. \quad (7)$$

In addition, for each of the three power sources, the control algorithm must provide limitation of the output current as well as assure that any of the multiple-input dc/dc power converter (MIPEC) input voltages do not drop down under a preset allowable value. Output voltage is constant at any given operating condition of the traction drive, and the demanded power is proportional to dc link current. Hence

$$P = V \cdot I \quad \rightarrow \quad \frac{dP}{dt} = V \cdot \frac{dI}{dt}. \quad (8)$$

Here

$$\boldsymbol{I}_{\text{link}} = \boldsymbol{I}_{\text{FC}} + \boldsymbol{I}_{\text{UC}} + \boldsymbol{I}_{\text{BU}} \quad (9)$$

$$\frac{dP_{\text{link}}}{dt} = V_{\text{link}} \cdot \frac{dI_{\text{link}}}{dt} \rightarrow \frac{dP_{\text{link}}}{dt} = V_{\text{link}} \left[ \frac{dI_{\text{FC}}}{dt} + \frac{dI_{\text{UC}}}{dt} + \frac{dI_{\text{BU}}}{dt} \right] \quad (10)$$

where $I_{\text{FC}}$, $I_{\text{UC}}$, and $I_{\text{BU}}$ are the current contributions of the three power sources to the MIPEC output current and

$$\left| \frac{dI_{\text{FC}}}{dt} \right| \le dI_{\text{FC max}} \quad 0 \le I_{\text{FC}} \le I_{\text{FC max}}$$

$$\left| \frac{dI_{\text{UC}}}{dt} \right| \le dI_{\text{UC max}} \quad |I_{\text{UC}}| \le I_{\text{UC max}}$$

$$\left| \frac{dI_{\text{BU}}}{dt} \right| \le dI_{\text{BU max}} \quad |I_{\text{BU}}| \le I_{\text{BU max}}. \quad (11)$$

The SOC values of battery and UC should remain within preset upper and lower bounds. This is achieved by regulating the current through a $P$ controller. In the voltage control loop, a hysteresis threshold around the desired dc link voltage is used to calculate the reference signal repetitive switching.

### B. Power Flow Management

The reference control signal for the RFC generator consists of the current required by the electric drive and the parameters that take into account the SOC values of battery and UC, respectively [10], [11].

For the recharging of the battery or the UC, the RFC generator changes its working point to supply the electric drive as well as to recharge the on-board energy storage devices. The expressions are given as follows:

$$I_{\text{FC}} = K_{\text{FC}} \cdot I_{\text{link}} + I_{\text{UCr}} \cdot K_{\text{UC.SOC}} + I_{\text{BUr}} \cdot K_{\text{BU.SOC}}$$

$$I_{\text{FC}} = K_{\text{FC}} \cdot (I_{\text{FC}} + I_{\text{UC}} + I_{\text{BU}}) + I_{\text{UCr}} \cdot K_{\text{UC.SOC}} + I_{\text{BUr}} \cdot K_{\text{BU.SOC}} \quad (12)$$

where $I_{\text{BUr}}$, $I_{\text{UCr}}$ are the recharging currents for battery and UC system, respectively, and are described by

$$I_{\text{BUr}} = \begin{cases} I_{\text{BUr}}, & \text{if SOC of BU} < 0.9 \\ 0, & \text{otherwise} \end{cases} \quad (13)$$

$$I_{\text{UCr}} = \begin{cases} I_{\text{UCr}}, & \text{if SOC of UC} < 0.8 \\ 0, & \text{otherwise.} \end{cases} \quad (14)$$

The rated power of the RFC generator system is typically 60% of the maximum power requested by the dc link. The RFC has to be shut off when the power consumption is less than 20% of its rated value, i.e.,

$$I_{\text{FC}} \le I_{\text{FC max}} = 0.61_{\text{link max}} = 0.6[I_{\text{FC max}} + I_{\text{UC max}} + I_{\text{BU max}}] \quad (15)$$

$$I_{\text{FC}} < 0.21_{\text{FC max}} \rightarrow I_{\text{FC}} = 0. \quad (16)$$

The reference control signal for the battery system is constant, to follow the electric drive specifications. The reference control signal for the UC consists of two parameters: the first one takes into account the UC SOC level and then either the required charging or discharging current. The second is proportional to the difference between the electric drive current request and the current supplied by the other energy sources. We have

$$I^*_{\text{UC}} = K_{\text{UCr}} \cdot I_{\text{UCr}} + K_{\text{UC}}(I_{\text{link}} - K_{\text{FC}} \cdot I_{\text{FC}}) \quad (17)$$

$$I^*_{\text{UC}} = K_{\text{UCr}} \cdot I_{\text{UCr}} + K_{\text{UC}}(I_{\text{FC}} + I_{\text{BU}} + I_{\text{UC}} - K_{\text{FC}} \cdot I_{\text{FC}}) \quad (18)$$

$$I^*_{\text{UC}} = K_{\text{UCr}} \cdot I_{\text{UCr}} + K_{\text{UC}} \left( I_{\text{BU}} + I_{\text{UC}} + (1 - K_{\text{FC}}) \cdot I_{\text{FC}} \right). \quad (19)$$

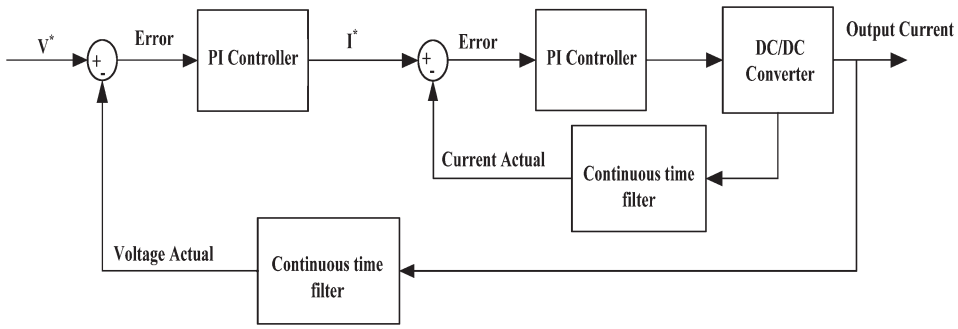


Fig. 3. UC control loop.

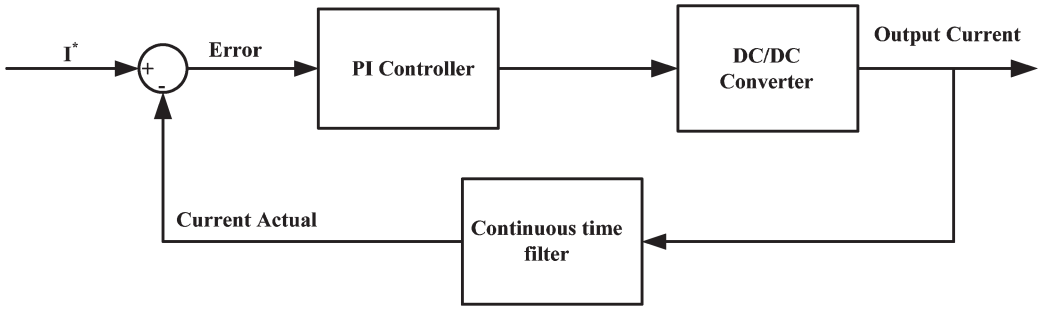


Fig. 4. RFC and battery (BU) control loop.

With this type of power flow management, the three power sources agree to supply the required output power, with the UC working to achieve slow current (power) time variations for both battery and RFC generator systems [10], [11].

The UC is dedicated to dc link voltage control. The outer voltage loop plus inner current loop is shown in Fig. 3. Fast control loops can greatly improve the entire system dynamic performance during load transients. In the UC power converter, switches operate in a complementary manner. Thus, the bidirectional converter compensates the dc link voltage unbalances in CCM operating mode.

To control each source current directly, current loops with $PI$-type regulators are used for both the RFC generator and battery power stage regulation, as depicted in Fig. 4. Complementary switching is used in the battery power converter to avoid discontinuous transitions from step-up to step-down mode of operation, and vice versa. By avoiding discontinuous transitions, reduction of current peaks is achieved, and both active and passive components are saved from dangerous stresses [7], [12], [13].

### C. System Simulation Procedure

An overview of the primary program loops is shown in Fig. 5. The outermost loop of the program selects different UC mass fractions at user defined intervals. The results provided use 10% mass fraction intervals, where "0" indicates BU mass and "1" indicates UC mass. Thus, a UC mass fraction of 0.4 indicates that 40% of the mass is UC and 60% of the mass is battery.

If a particular amount of mass is capable of completing the power profile, then the program decreases the total mass. If a

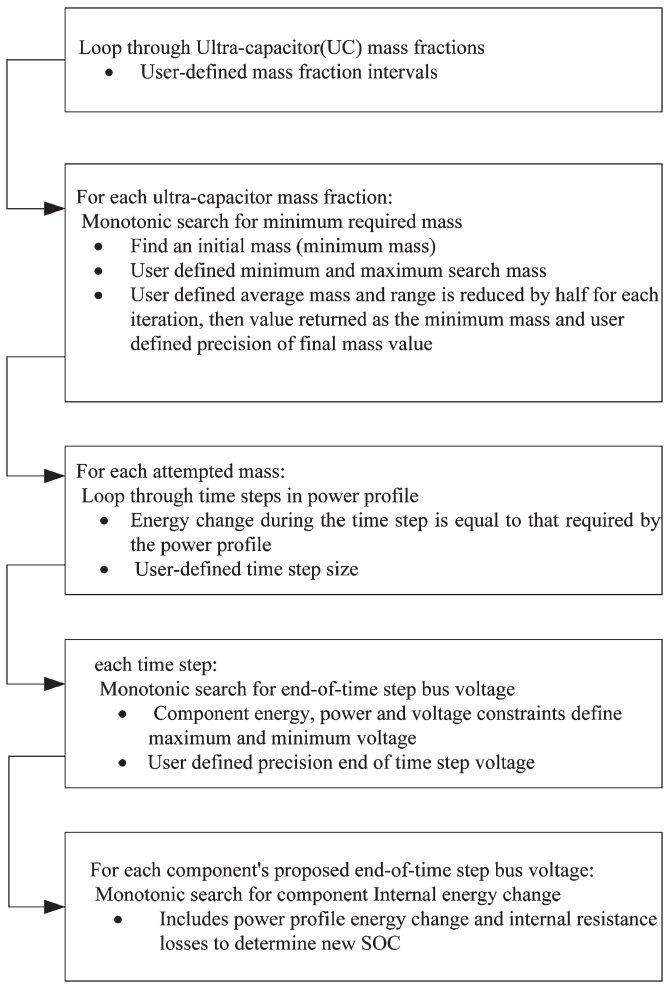


Fig. 5. Nested loop overview for simulation software.

mass value is not capable of completing the drive cycle, then the total mass is increased. This continues until the minimum required mass is known within a user-defined range. Because there are no local minima, it can be searched within a range of values, and we can be certain that this minimum value is the only minimum. The monotonic search (the technique used to adjust the minimum mass) uses an initial range and tests the maximum and minimum allowable masses. The average mass is then tested and is used as the new minimum or maximum, depending on the results of the test. This way, the overall range is reduced by half. When the range is smaller than the required mass precision, the value is returned as the minimum mass. For a particular mass and ratio, the power profile is traversed as a series of time steps. Within an individual time step, energy is transferred between the battery and UC such that the net energy change during the time step is equal to that required by the power profile. SOC information from the previous time step is used as a starting point.

In the case of passively connected battery and UC, there is an additional constraint that the bus voltage at the end of each time step is equal for the battery and UC. It is obvious that the method of determining the power flows is similar to the method of determining minimum mass; for a particular final bus voltage, there are average power flows that must occur during the time step.

Using a range of allowable voltage, the end-of-time step voltage is iteratively calculated to within a user-defined precision. If the constraints (power, energy, and voltage) create a situation, wherein the demands of the power profile cannot be met, the initial mass assumption is deemed insufficient. The total mass is incremented, and the power profile is reset to the initial time [14], [15].

### D. Battery and UC Modeling

Resistance-based models of the batteries and UCs represent an SOC-dependent voltage source in series with a resistor. The power constraints, available energy, volume, and cost are all directly scaled to the mass. The internal resistance $(R_{\text{int}})$ calculation is dependent on the energy and voltage. For a constant amount of battery material, a higher $V_{\max}$ results in a higher $R_{\text{int}}$ (series-connected cells). Conversely, a lower $V_{\max}$ results in a lower $R_{\text{int}}$ (parallel-connected cells). Hence, the energy or mass relation is direct. Resistance factor is calculated using

$$R_{\text{factor}} = \frac{R_{\text{int}} \cdot E_{\max}}{V_{\max}^2}. \tag{20}$$

The $R_{\text{int}}$ for a known amount of battery or UC is determined by

$$R_{\text{int}} = \frac{R_{\text{factor}} \cdot V_{\max}^2}{E_{\max}}. \tag{21}$$

The $R_{\text{int}}$ is responsible for voltage fluctuations away from the open-circuit voltage during charging and discharging. These voltage fluctuations allow UCs to handle large amounts of energy in passively connected systems, which can result in extended battery life and reduction of mass. The battery maximum energy can be estimated as

$$\text{Energy}_{\max,\text{BU}} = \frac{Ah_{\max} \cdot V_{\text{nom}} \cdot 3600 \text{ s/h}}{1000 \text{ J/kJ}}. \tag{22}$$

This quantity of BU represents the theoretical short-circuit discharge time (SCDT). If a BU could be short circuited without damaging itself, it would take a certain amount of time to fully discharge all of the stored energy, which depends on the energy capacity $V_{\text{nom}}$ and $R_{\text{int}}$ of the battery. The SCDT is only dependent on the battery technology and allows comparison of $R_{\text{int}}$ between dissimilar battery types or comparison of the same battery type from different manufacturers [15]. The SCDT is determined by

$$\text{SCDT} = \frac{R_{\text{int}} \cdot E_{\max}}{V_{\text{nom}}^2}. \tag{23}$$

SOCs of UC curves are based on the $E = CV^2$ profile, as shown in Fig. 6, for a 600-F UC.

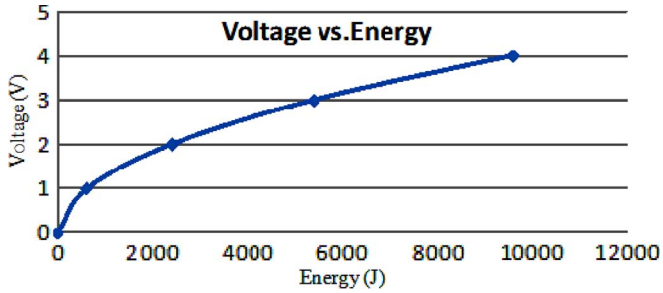


Fig. 6. Voltage versus energy for a 600-F UC.

### E. Control Strategies With Advisor Model

The Advanced Vehicle Simulator (ADVISOR) software, working in a Matlab/Simulink environment, is used for the parallel combination of the battery and UC. Table I summarizes the three basic modes of operation of the parallel energy source.

Both the battery and the UC can be charging or discharging at the same time; the battery can discharge while supplying power to the motor and UC. A proper control strategy for the energy source is hard to determine. The control strategy used for the battery is to maintain the SOC between 60% and 70% of its maximum capacity based on ADVISOR's standard for a parallel drive train [16], [17].

The SOC is calculated by ADVISOR according to the characteristics of the energy source. The UC is controlled through the dc/dc converter shown in Fig. 7. The converter receives a demand for power from the vehicle, either positive to demand power from the source or negative to supply regenerative power to the source. If the power demand is less than zero (mode III in Table I), the converter will proportionally send power to the battery and UC for charging relative to the SOC of each component.

TABLE I
MODES OF OPERATION OF DC/DC CONVERTER

| Mode | Power Source | Load | Operation | Brief Explanation of Operation |
|---|---|---|---|---|
| 1 | Battery and UC | Motor | Boost of Power | UC supplies power up to the limits of the converter. BU supplies the rest of the power needed. |
| 2 | Battery | UC &Motor | Lower motor demands | Demands of the electrical loads are low so the battery can supply power to the motor and charge the UC if needed. |
| 3 | Motor (Generator) | UC & Battery | Regeneration brake | UC Fully charge and BU take whatever power is left or until regeneration is over with. |

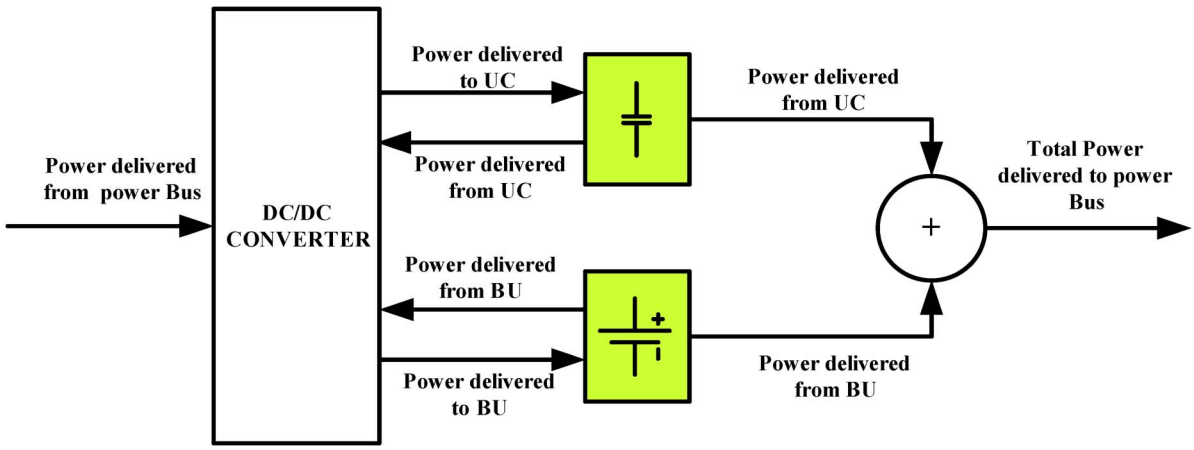


Fig. 7. Block diagram model programmed in Simulink.

TABLE II
VALUE OF $K$ AT DIFFERENT UC SOCS

| SOC of UC | 0 | 0.4 | 0.5 | 0.6 | 1 |
|---|---|---|---|---|---|
| K(W) | 40000 | 40000 | 10000 | 0 | 0 |

In case of demand of power from the energy source for the vehicle, two modes have to be accounted for. To do this, a dynamic variable $K$ is created. $K$ is the power requested (in watts) from the battery and UC at various SOCs of the UC. Table II shows the value of different SOCs of UC in terms of the value of $K$. The $K$ variable is changed to achieve maximum performance and fuel economy. With this arrangement, modes I and II in Table I can be achieved. If the power demand from the vehicle is greater than $K$, the converter is in mode I; therefore, if the power demand from the vehicle is less than $K$, the converter is in mode II [17].

The hybridization factor is defined as the power of the electrical propulsion system ($P_{\text{motor}}$) divided by the total power of the vehicle [16], [17], i.e.,

$$\text{HF} = \frac{P_{\text{motor}}}{P_{\text{motor}} + P_{\text{ICE}}} \tag{24}$$

$$P_{\text{Total}} = P_{\text{motor}} + P_{\text{ICE}}. \tag{25}$$

## III. COMPARISON OF BIDIRECTIONAL DC/DC CONVERTER TOPOLOGIES

In this section, the operational characteristics of four popularly proposed ESS converters are compared. These include buck–boost, half-bridge, Cuk, and the combined SEPIC and Luo converters. The bidirectional converter is used as the power electronics interface of a UC pack (requiring boost operation in one direction of power flow and buck operation in another direction) and restricts the peak voltage to lower than or equal to the dc bus voltage. Buck–boost and half-bridge converters are similar because the buck–boost converter has active and passive components with lower electric and thermal stresses and need twice the number of active components. The half-bridge converter has same number of active and passive components as the two-quadrant buck–boost converter. Fig. 8 depicts the buck–boost and half-bridge converter topologies for EV/PHEV ESS applications.

The half-bridge converter operates as follows: When power flows from UC pack (input capacitor) to dc bus, $S_1 =$ on, $D_1 =$ on and $S_2 =$ off, $D_2 =$ off, representing a boost converter, and when power flows from the HV dc bus to the UC pack, $S_2 =$ on, $D_2 =$ on and $S_1 =$ off, $D_1 =$ off, and it operates as a buck converter. The third converter is the Cuk converter, as shown in Fig. 9. When power flows from the UC pack to the dc bus, the converter operates in the boost mode, whereby $S_1 =$ on,

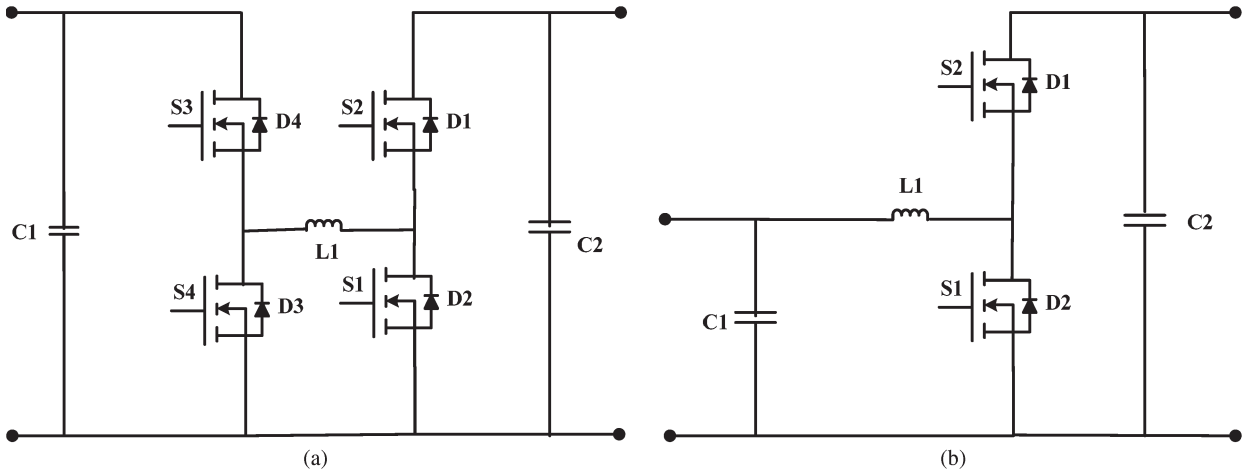


Fig. 8. (a) Cascaded buck–boost converter. (b) Half-bridge converter.

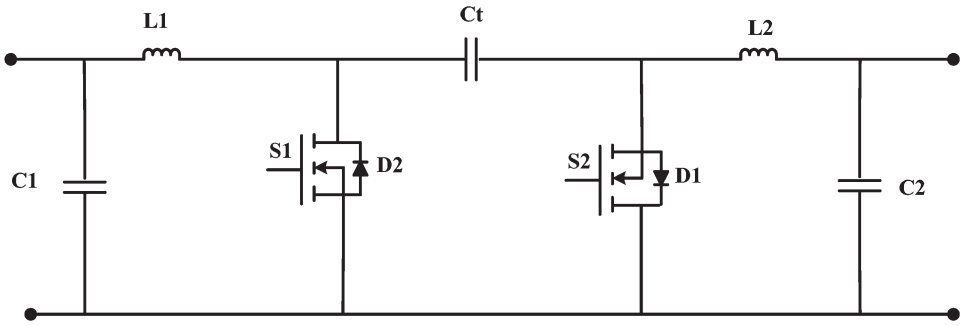


Fig. 9. Cuk converter for PHEV energy storage applications.

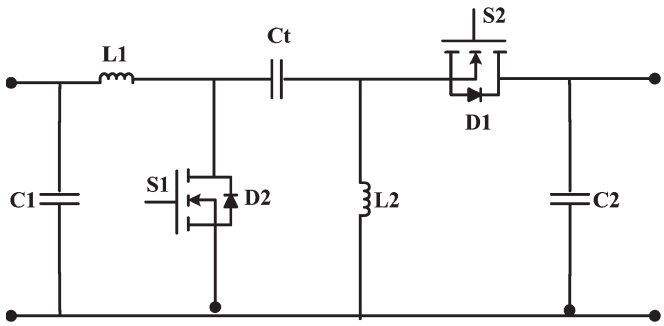


Fig. 10. Combined SEPIC and Luo converter.

$D_1 =$ on and $S_2 =$ off, $D_2 =$ off. In the buck mode, power flows from the dc bus to the UC, and $S_2 =$ on, $D_2 =$ on and $S_1 =$ off, $D_1 =$ off.

Another popular converter topology combines the SEPIC and Luo converters (Fig. 10). The SEPIC converter boosts the voltage when power flows from the UC pack to the dc bus. Hence, $S_1 =$ on, $D_1 =$ on and $S_2 =$ off, $D_2 =$ off. The Luo converter bucks the voltage down when power flows from the dc bus to the UC pack, and $S_2 =$ on, $D_2 =$ on and $S_1 =$ off, $D_1 =$ off.

For obtaining the inductor size, the following two factors are important: 1) inductor average current $I_{L,\mathrm{dc}}$, since it determines the wire size and is related to the maximum load current $I_O$, and 2) inductor current ripple $\Delta I_L$, since it is responsible for the core loss and determines the peak inductor current $I_{L,\mathrm{peak}} = (I_{L,\mathrm{dc}} + \Delta I_L)$. Peak inductor current determines inductor energy $(0.5LI^2_{L,\mathrm{peak}})$. Inductor current ripple ratio is given by $r_{l=(\Delta I_L/I_{L,\mathrm{dc}})}$. For obtaining the size of the capacitors, the following three factors are important: 1) capacitor rms current value $(I_{C,\mathrm{rms}})$, which determines the capacitor loss (ESR $\times\, I^2_{C,\mathrm{rms}}$); 2) peak-to-peak capacitor current $I_{C,\mathrm{pp}}$ that determines the capacitor voltage, $V_C$; and 3) capacitor voltage ripple ratio $r_{c=(\Delta V_C/V_{C,\mathrm{avg}})}$, where $\Delta V_C$ is the capacitor voltage ripple.

With constant switching frequency and output power, the energy stored in the inductor is $(1 + r_l)^2/r_L$, the energy stored in the capacitor is $(1 + r_C)^2/r_C$, and the cost and size of the passive components are dependent on the energy stored. Inductors for all types of converters have approximately the same energy requirement. It is interesting to note the following differences between the half-bridge, Cuk, and combined SEPIC and Luo converters.

1) The duty cycle of the half-bridge converter is higher than Luo and Cuk during boost mode (when UC pack is being charged) with the same voltage ratio $V_o/V_i$, and the duty cycle of the half-bridge converter is lower than that of the Cuk and SEPIC in buck mode (UC pack being discharged) with the same voltage ratio $(V_o/V_i)$.

2) The rms current of $L_2$ in Cuk and combined SEPIC and Luo converters is almost constant. Furthermore, the conduction losses are also almost constant. The rms current of $L_1$ in half-bridge, Cuk, and combined Luo and SEPIC converters increases when operating at the voltage ratio $V_o/V_i$ closer to end values and conduction losses of inductor $L_1$ are higher than those of inductor $L_2$, whereby $L_1$ and $L_2$ have the same inductance value and the same energy requirements. Heat dissipation is more critical for $L_1$ than for $L_2$, and this fact has a negative impact on the efficiencies of the Cuk and combined SEPIC and Luo converters. This is because these converters require two inductors instead of one.
3) Switch and diode peak currents for Cuk and combined Luo and SEPIC converters are higher than the diode and switch peak currents of the half-bridge configuration.
4) The rms current value of the active component determines conduction losses. The switch and diode rms currents of the half-bridge converter are lower than those of the Cuk and combined Luo and SEPIC converters. In addition, the conduction losses for active components of the half-bridge converter are lower than those of the Cuk and combined Luo and SEPIC configurations, eventually improving their round-trip efficiency.
5) The rms current of the output capacitor in the half-bridge converter (as well as the SEPIC in boost operation mode) is greater than the rms current of the output capacitor of the half-bridge, Cuk, and Luo converters that operate in buck mode. As a result, the peak current of the output capacitor of the half-bridge and SEPIC converters in boost operating mode is larger than the peak current of the output capacitor of half-bridge, Cuk, and Luo converters in buck operating mode. Therefore, energy requirements for the output capacitor are greater.

Then main advantages and disadvantages of the half-bridge, Cuk, and combined Luo and SEPIC converters can be summarized as follows. In the half-bridge converter, there is only one inductor instead of two. The size of the inductor in the half-bridge converter is only half the size of that in the Cuk and combined Luo and SEPIC converters. Furthermore, the half-bridge converter has higher efficiencies than the Cuk, Luo, and SEPIC converters because it has lower inductor conduction and switching losses for the active component. The inductor of the half-bridge converter and $L_1$ (input inductor) in the Cuk and combined Luo and SEPIC converters have the same energy requirements and have approximately the same core and the same conduction losses. The major disadvantage of the half-bridge converter is its discontinuous output current when operating in boost mode. This impacts the size of the output capacitor.

The main advantage of the Cuk converter is its reduced input and output current ripple, with the possibility of ripple-free current when integrating the inductances. The disadvantage of the Cuk converter is its large inductors and the fact that the transfer capacitor has to be rated at $V_i + V_o$. The main advantage of the combined Luo and SEPIC converter is that the transfer capacitor is rated only to $V_i$, while the disadvantage of this converter includes the usage of two large inductors. Moreover, the output capacitor is large and the output current is discontinuous [18].

## IV. Conclusion and Future Work

In this paper, the concept of a MIPEC, which is devoted to combine the power flows of multiple energy sources of the on-board EV/PHEV ESS, has been presented. Furthermore, this paper mainly focused on providing a comprehensive review of control system architectures for popularly adopted MIPEC and bidirectional dc/dc converters for EV/PHEV ESS applications.

A hybrid arrangement, with a parallel combination of batteries and UCs, can significantly reduce the volume and weight of the overall EV ESS. Furthermore, overall battery life can be drastically improved due to the decrease in the output current. In addition, a hybrid energy storage arrangement enhances the temperature adaptability and may also simplify the overall energy management strategy. Future work in this area of research will aim at addressing the comparison and different combinations of UC and battery systems to reduce the size and cost, with a cosimulated usage of the popular ADVISOR vehicle simulation software and computer-aided-design-intensive power electronics modeling software.

## References

[1] S. K. Biradar, R. A. Patil, and M. Ullegaddi, "Energy storage system in electric vehicle," in *Proc. IEEE Power Quality*, 1998, pp. 247–255.
[2] X. Yan and D. Patterson, "Improvement of drive range, acceleration and deceleration performances in an electric vehicle propulsion system," in *Proc. IEEE Power Electron. Spec. Conf.*, Jun. 1999, vol. 2, pp. 638–643.
[3] S. M. Lukic, S. G. Wirasingha, F. Rodriguez, J. Cao, and A. Emadi, "Power management of an ultra-capacitor/battery hybrid energy storage system in an HEV," in *Proc. IEEE Vehicle Power Propuls. Conf.*, Sep. 2006, pp. 1–6.
[4] J. Moreno, M. E. Ortuzar, and J. W. Dixon, "Energy-management system for a hybrid electric vehicle, using ultracapacitors and neural networks," *IEEE Trans. Ind. Electron.*, vol. 53, no. 2, pp. 614–623, Apr. 2006.
[5] M. E. Ortuzar, J. Moreno, and J. W. Dixon, "Ultracapacitor-based auxiliary energy system for an electric vehicle: Implementation and evaluation," *IEEE Trans. Ind. Electron.*, vol. 54, no. 4, pp. 2147–2156, Aug. 2007.
[6] C. A. Ramos-Paja, C. Bordons, A. Romero, R. Giral, and L. Martinez-Salamero, "Minimum fuel consumption strategy for PEM fuel cells," *IEEE Trans. Ind. Electron.*, vol. 56, no. 3, pp. 685–696, Mar. 2009.
[7] A. Lidozzi and L. Solero, "Power balance control of multiple-input DC–DC power converter for hybrid vehicles," in *Proc. IEEE Int. Symp. Ind. Electron.*, May 2004, pp. 1467–1472.
[8] H. Matsuo, W. Lin, F. Kurokawa, T. Shigemizu, and N. Watanabe, "Characteristics of the multiple-input DC–DC converter," *IEEE Trans. Ind. Electron.*, vol. 51, no. 3, pp. 625–631, Jun. 2004.
[9] A. Di Napoli, F. Crescimbini, S. Rodo, and L. Solero, "Multiple input DC–DC power converter for fuel-cell powered hybrid vehicles," in *Proc. IEEE Power Electron. Spec. Conf.*, Jun. 2002, vol. 4, pp. 1685–1690.
[10] M. H. Todorovic, L. Palma, and P. N. Enjeti, "Design of a wide input range DC–DC converter with a robust power control scheme suitable for fuel cell power conversion," *IEEE Trans. Ind. Electron.*, vol. 55, no. 3, pp. 1247–1255, Mar. 2008.
[11] A. Emadi, Y. J. Lee, and K. Rajashekara, "Power electronics and motor drives in electric, hybrid electric, and plug-in hybrid electric vehicles," *IEEE Trans. Ind. Electron.*, vol. 55, no. 6, pp. 2237–2245, Jun. 2008.
[12] Y. M. Chen, Y. C. Liu, and S. H. Lin, "Double-input PWM DC–DC converter for high/low voltage sources," in *Proc. IEEE Int. Telecommun. Energy Conf.*, Oct. 2003, pp. 27–32.

[13] K. P. Yalamanchili and M. Ferdowsi, "Review of multiple input DC–DC converters for electric and hybrid vehicles," in *Proc. IEEE Vehicle Power Propuls. Conf.*, Sep. 2005, pp. 160–163.
[14] A. Emadi, S. S. Williamson, and A. Khaligh, "Power electronics intensive solutions for advanced electric, hybrid electric, and fuel cell vehicular power systems," *IEEE Trans. Power Electron.*, vol. 21, no. 3, pp. 567–577, May 2006.
[15] S. M. Lukic, J. Cao, R. C. Bansal, F. Rodriguez, and A. Emadi, "Energy storage systems for automotive applications," *IEEE Trans. Ind. Electron.*, vol. 55, no. 6, pp. 2258–2267, Jun. 2008.
[16] S. Williamson, S. M. Lukic, and A. Emadi, "Comprehensive drive train efficiency analysis of hybrid electric and fuel cell vehicles based on motor-controller efficiency modeling," *IEEE Trans. Power Electron.*, vol. 21, no. 3, pp. 730–740, May 2006.
[17] Z. Jiang and R. A. Dougal, "A compact digitally controlled fuel cell/battery hybrid power source," *IEEE Trans. Ind. Electron.*, vol. 53, no. 4, pp. 1094–1104, Jun. 2006.
[18] K. Stricklett, *Advanced Components for Electric and Hybrid Electric Vehicles*. Springfield, VA: NIST Special Publication.

**Zahra Amjadi** (S'08) received the B.E. degree in electrical engineering in 2003 from Azad University, Tehran, Iran, and the M.A.Sc. degree in electrical engineering in 2007 from Concordia University, Montreal, Canada, where she has been working toward the Ph.D. degree, specializing in automotive power electronics, with the Power Electronics and Energy Research Group, Department of Electrical and Computer Engineering, since January 2008.

Her research interests include power-electronics-based energy management techniques for hybrid electric vehicle energy storage systems.

**Sheldon S. Williamson** (S'01–M'06) received the B.E. degree in electrical engineering (with high distinction) from the University of Mumbai, Mumbai, India, in 1999, and the M.S. and Ph.D. (with honors) degrees in electrical engineering from the Illinois Institute of Technology, Chicago, with specialization in automotive power electronics and motor drives, in 2002 and 2006, respectively.

Since June 2006, he has been an Assistant Professor with the Department of Electrical and Computer Engineering, Concordia University, Montreal, Canada, where he is currently with the Power Electronics and Energy Research Group. He is the principal author or a coauthor of over 60 journal and conference papers. He is also the author of four chapters in the book *Vehicular Electric Power Systems* (Marcel Dekker, 2003). He is also the author of two chapters in the book *Energy Efficient Electric Motors* (CRC, 2004). His main research interests include the study and analysis of electric drive trains for electric, hybrid electric, plug-in hybrid electric, and fuel cell vehicles. His research interests also include modeling, analysis, design, and control of power electronic converters and motor drives for land, sea, air, and space vehicles, as well as power electronic interfaces and control of renewable energy systems.

Dr. Williamson serves as a Chapter Chair for the IEEE Montreal section of the IEEE Industry Applications Society and the IEEE Power Engineering Society. He is also a Member of the IEEE Power Electronics Society (PELS), the IEEE Industrial Electronics Society, and the IEEE Vehicular Technology Society. He has offered numerous conference tutorials, lectures, and short courses in the areas of automotive power electronics and motor drives. In addition, he has been selected as the General Chair for the IEEE Vehicle Power and Propulsion Conference, to be held in Montreal, in September 2013. He was also selected as the Technical Program Chair of the IEEE Canada Electrical Power and Energy Conference, to be held in Montreal, in October 2009. He also served as the Project Coordination and Awards Chair at the 2007 IEEE Canada Electrical Power Conference, Montreal. He was the Conference Secretary for the 2005 IEEE Vehicle Power and Propulsion Conference, Chicago, IL. He is also the recipient of numerous awards and recognitions. He has the honor of being included in the prestigious *International Who's Who of Professionals* and the *International Who's Who in Engineering Higher Education*. He was also the recipient of the prestigious "Paper of the Year" Award in the field of automotive power electronics from the IEEE Vehicular Technology Society (IEEE VTS) in 2006. In addition, he also received the overall "Best Paper" Award at the IEEE PELS and VTS Cosponsored Vehicle Power and Propulsion Conference in September 2007. He also received the prestigious Sigma Xi/IIT Award for Excellence in University Research for the academic year 2005–2006. In 2006, he also received the "Best Research Student" Award, Ph.D. category, within the Department of Electrical and Computer Engineering, Illinois Institute of Technology, Chicago.